

# Impurity effect and suppression to superconductivity in $\text{Na}(\text{Fe}_{0.97-x}\text{Co}_{0.03}\text{T}_x)\text{As}$ ( $\text{T}=\text{Cu}, \text{Mn}$ )

Qiang Deng, Xiaxin Ding, Sheng Li, Jian Tao, Huan Yang, Hai-Hu Wen\*

*Center for Superconducting Physics and Materials,*

*National Laboratory of Solid State Microstructures and Department of Physics, Nanjing University, Nanjing 210093, China*

We report the successful growth and the impurity scattering effect of single crystals of  $\text{Na}(\text{Fe}_{0.97-x}\text{Co}_{0.03}\text{T}_x)\text{As}$  ( $\text{T}=\text{Cu}, \text{Mn}$ ). The temperature dependence of DC magnetization at high magnetic fields is measured for different concentrations of Cu and Mn. Detailed analysis based on the Curie-Weiss law indicates that the Cu doping weakens the average magnetic moments, while doping Mn enhances the local magnetic moments greatly, suggesting that the former may be non- or very weak magnetic impurities, and the latter give rise to magnetic impurities. However, it is found that both doping Cu and Mn will enhance the residual resistivity and suppress the superconductivity at the same rate in the low doping region, being consistent with the prediction of the  $S^\pm$  model. For the Cu-doped system, the superconductivity is suppressed completely at a residual resistivity  $\rho_0 = 0.87 \text{ m}\Omega \text{ cm}$  at which a strong localization effect is observed. However, in the case of Mn doping, the behavior of suppression to  $T_c$  changes from a fast speed to a slow one and keeps superconductive even up to a residual resistivity of  $2.86 \text{ m}\Omega \text{ cm}$ . Clearly the magnetic Mn impurities are even not as detrimental as the non- or very weak magnetic Cu impurities to superconductivity in the high doping regime.

PACS numbers: 74.20.Rp, 74.70.Dd, 74.62.Dh, 74.70.Xa

## I. INTRODUCTION

The discovery of iron-based superconductors in 2008 has brought about new vigor and vitality into the study of unconventional superconductivity.<sup>1</sup> The pairing symmetry is very crucial for understanding the superconducting mechanism. In the cuprates, the pairing symmetry was proved to be d-wave,<sup>2</sup> while in the iron-based superconductors it is still under debate. Theoretically, a pairing model with the gap structure of  $S^\pm$  was proposed. This model is based on the assumption that the pairing is established by exchanging the paramagnons given by the antiferromagnetic spin fluctuations between two electrons with opposite momentum and spins. This kind of pairing will naturally lead to a sign reversal of the order parameter between the electron and the hole Fermi pockets.<sup>3-7</sup> This model has gained supports from many experiments, including the scanning tunneling spectroscopy (STS) measurements<sup>8,9</sup> and inelastic neutron scattering experiments.<sup>10</sup> On the other hand, a pairing state without the sign reversal of the gaps, namely  $S^{++}$ , was proposed if the pairing is mediated by orbital fluctuations.<sup>11-13</sup> In some special cases, even the d-wave gap may be expected in iron-based superconductors.<sup>4,14,15</sup>

In the superconducting state, the impurity scattering effect is closely related to the gap structure, the characteristics of the impurities and the underlying electronic structure. The impurity scattering effect may give some important clues to unravel the pairing gap structure as well as the pairing mechanism. According to the Anderson's theorem,<sup>16</sup> in a conventional s-wave superconductor, the magnetic impurity can break the Cooper pairs easily, while superconductivity remains robustly with the presence of nonmagnetic impurities in the unitary limit.

In sharp contrast, Anderson's theorem is seriously violated for the unconventional superconductor, where both magnetic and nonmagnetic impurities are detrimental to superconductivity. In cuprate superconductors with a d-wave gap structure, significant  $T_c$  suppression was observed with doping Zn.<sup>17-19</sup> In the case of  $S^\pm$  pairing state, it was pointed out that both magnetic and nonmagnetic impurities can suppress  $T_c$  rapidly.<sup>11,20,21</sup> In order to unveil the mystery of superconducting mechanism, plenty of experiments have been carried out on the impurity effects in iron-based superconductors.<sup>7,22-34</sup> Unfortunately, the conclusions remain highly controversial. Previous studies on Mn impurities showed that  $T_c$  was strongly suppressed in  $\text{Ba}_{0.5}\text{K}_{0.5}\text{Fe}_2\text{As}_2$ <sup>22,24</sup> and  $\text{Ba}(\text{Fe}_{1-y}\text{Co}_y)_2\text{As}_2$  system,<sup>25</sup> while  $T_c$  is not suppressed or even enhanced in Mn-doped  $\text{FeSe}_{0.5}\text{Te}_{0.5}$  superconductor.<sup>27</sup> Zn impurity suppress  $T_c$  rapidly in  $\text{BaFe}_{1.89-2x}\text{Zn}_{2x}\text{Co}_{0.11}\text{As}_2$ ,<sup>26</sup> whereas superconducting state remains robustly in  $\text{Fe}_{1-y}\text{Zn}_y\text{Se}_{0.3}\text{Te}_{0.7}$ .<sup>28</sup> Theoretically it is proposed that the pairing symmetry in iron-based superconductor can be different from material to material.<sup>7</sup> A study in  $\text{LaFe}_{1-y}\text{Zn}_y\text{AsO}_{1-x}\text{F}_x$  system showed that superconducting transition temperature increases in the underdoped regime with doping Zn impurities, remains unchanged in the optimally doped regime and severely suppressed in the overdoped regime, suggesting that the pairing symmetry could change from S-wave to  $S^\pm$  or even d-wave states with increasing doping concentration.<sup>29</sup> In order to have a better understanding of the pairing symmetry and superconducting mechanism in Fe-based superconductors, further experimental studies, especially with the known properties of the impurities, are highly desired.

In this study, we investigate the impurity effect of doping Cu and Mn into the 111-type iron-based supercon-

ductors  $\text{Na}(\text{Fe}_{0.97}\text{Co}_{0.03})\text{As}$ . Our study reveal that the Cu doping weakens the average magnetic moments (below  $0.4 \mu_B/\text{Fe}$  site), while doping Mn enhances the local magnetic moments greatly, suggesting that Cu dopants behave as non- or very weak magnetic impurities, and Mn dopants are magnetic ones. It is found that both doping Cu and Mn can enhance the residual resistivity and suppress the superconductivity rapidly, which is consistent with the prediction of the  $S^\pm$  pairing model in the low doping region.

## II. EXPERIMENTAL METHODS

The single crystals of  $\text{Na}(\text{Fe}_{0.97}\text{Co}_{0.03})\text{As}$  (named as pristine sample) and  $\text{Na}(\text{Fe}_{0.97-x}\text{Co}_{0.03}\text{T}_x)\text{As}$  ( $\text{T} = \text{Cu}$  and  $\text{Mn}$ ) were synthesized by the self-flux method using  $\text{NaAs}$  as the flux. Firstly,  $\text{NaAs}$  was prepared as the precursor. The  $\text{Na}$  (purity 99%, Alfa Aesar) was cut into pieces and mixed with  $\text{As}$  powders (purity 99.99%, Alfa Aesar), the mixture was put into an alumina crucible and sealed in a quartz tube in vacuum. Then it was slowly heated up to  $200^\circ\text{C}$  and held for 10 hours, followed by cooling down to room temperature. Then the resultant  $\text{NaAs}$ , and  $\text{Fe}$  (purity 99.9%, Alfa Aesar),  $\text{Co}$  (purity 99.9%, Alfa Aesar),  $\text{Cu}$  or  $\text{Mn}$  (purity 99.9%, Alfa Aesar) powders were weighed with an atomic ratio of  $\text{NaAs}:\text{Fe}:\text{Co}:\text{T} = 4:(0.97-x):0.03:x$  and ground thoroughly. The mixture was loaded into an alumina crucible, then sealed in an iron tube under  $\text{Ar}$  atmosphere. The iron tube was then sealed in an evacuated quartz tube to prevent the oxidization of the iron tube. Then it was placed into the furnace and heated up to  $950^\circ\text{C}$  and held for 10 hours, followed by cooling down to  $600^\circ\text{C}$  at a rate of  $3^\circ\text{C}/\text{h}$  to grow single crystals. Single crystals with shiny surfaces and typical dimensions of  $5\text{mm}\times 5\text{mm}\times 0.2\text{mm}$  were obtained. In the preparation process, the weighing, mixing, grinding were conducted in a glove box under argon atmosphere with the  $\text{O}_2$  and  $\text{H}_2\text{O}$  below 0.1 PPM. The x-ray diffraction (XRD) measurements were performed on a Bruker D8 Advanced diffractometer with the  $\text{Cu-K}_\alpha$  radiation. The DC magnetization measurements were carried out with a SQUID-VSM-7T (Quantum Design). The in-plane resistivity measurements were done on a PPMS-16T (Quantum Design) with the standard four-probe method.

## III. RESULTS AND DISCUSSION

### A. X-ray diffraction

Fig. 1 shows the XRD patterns of the  $\text{Na}(\text{Fe}_{0.97-x}\text{Co}_{0.03}\text{T}_x)\text{As}$  ( $\text{T}=\text{Cu}$ ,  $\text{Mn}$ ) single crystals. Only  $(00l)$  peaks can be observed, and all the diffraction peaks show a full width at half maximum (FWHM) less than  $0.05^\circ$ , indicating that the cleavage plane is the  $ab$  plane and the high quality of the samples.

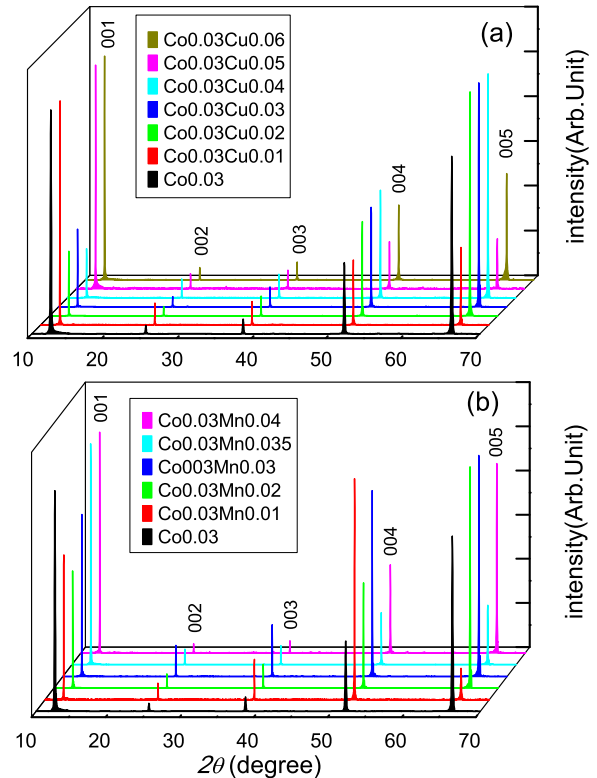


FIG. 1: (color online) The XRD patterns of (a)  $\text{Na}(\text{Fe}_{0.97-x}\text{Co}_{0.03}\text{Cu}_x)\text{As}$ , and (b)  $\text{Na}(\text{Fe}_{0.97-x}\text{Co}_{0.03}\text{Mn}_x)\text{As}$  single crystals.

As shown in Fig. 2(a) and (b), peaks of the  $(004)$  reflection shift monotonously in  $2\theta$  with the increase of doping concentration, indicating that the impurities were doped into the crystal lattice successfully. This conclusion is also supported by the monotonic increase of the residual resistivity versus doping level in both systems. The lattice parameter of  $c$ -axis is obtained and plotted as a function of doping concentration  $x$ , as shown in Fig. 2(c). For the pristine sample, the lattice parameter of  $c$ -axis is  $7.048 \text{ \AA}$ , which is consistent with the previously reported results within experimental error.<sup>35</sup> We can see that, the  $c$ -axis lattice parameter slightly increases with the increase of Mn doping concentration, while it decreases in the Cu-doped samples. This behavior is similar to the results in other reports.<sup>24,33</sup>

### B. Magnetization and resistivity measurements

In Fig. 3, we present the temperature dependence of the in-plane resistivity from 2 K to 300 K for  $\text{Na}(\text{Fe}_{0.97-x}\text{Co}_{0.03}\text{Cu}_x)\text{As}$  single crystals. Obviously,  $T_c$  goes down and the residual resistivity goes up with the

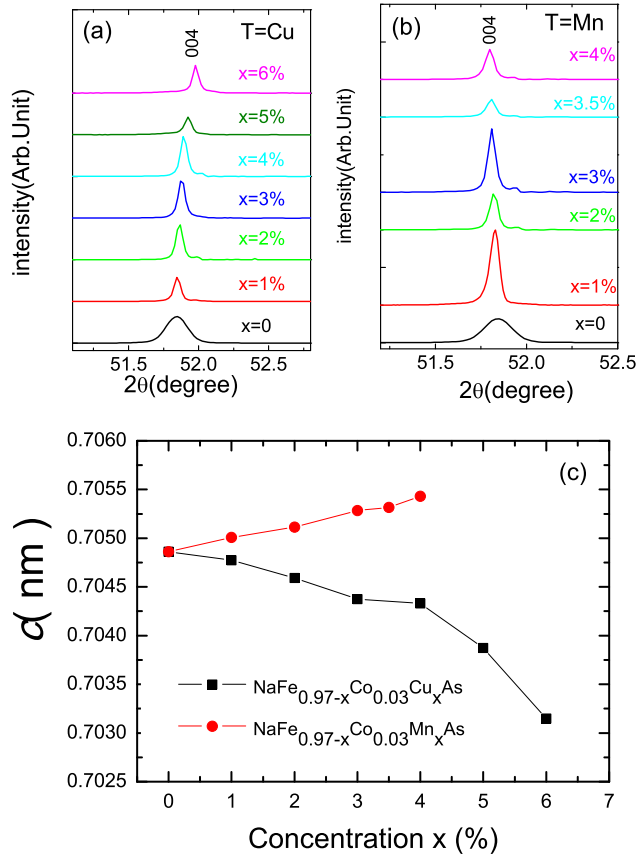


FIG. 2: (color online) (a) and (b) Peaks of the (004) reflections of  $\text{Na}(\text{Fe}_{0.97-x}\text{Co}_{0.03}\text{T}_x)\text{As}$  ( $\text{T} = \text{Cu}$  and  $\text{Mn}$ ) single crystals. (c) The lattice parameter of c-axis plotted as a function of the doping concentration  $x$  for Cu and Mn doped samples.

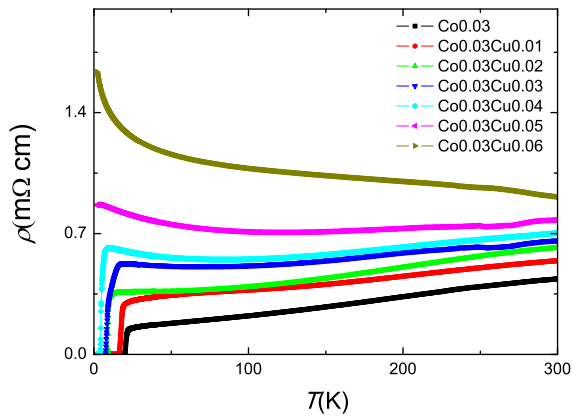


FIG. 3: (color online) Temperature dependence of the in-plane resistivity of  $\text{Na}(\text{Fe}_{0.97-x}\text{Co}_{0.03}\text{Cu}_x)\text{As}$ .

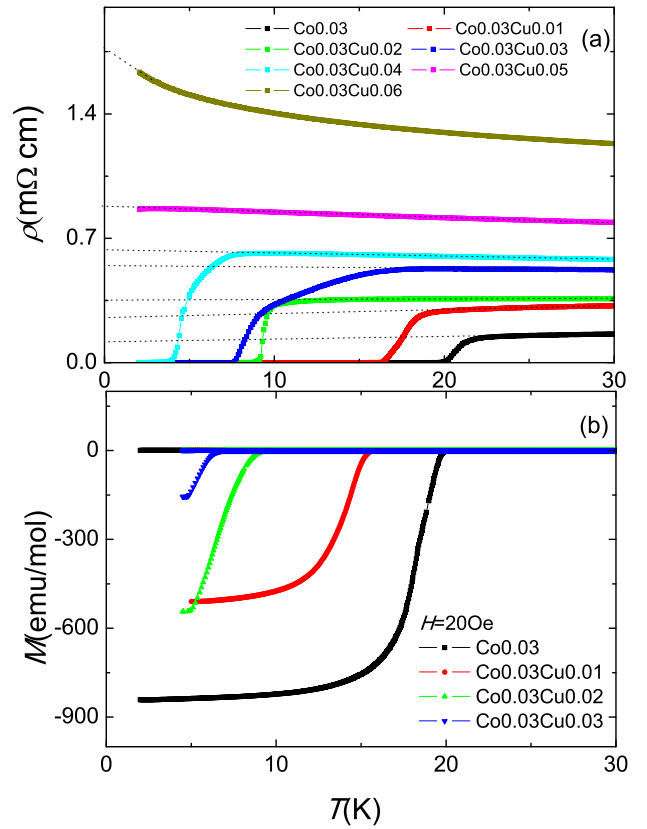


FIG. 4: (color online) (a) Temperature dependence of resistivity in low temperature region for  $\text{Na}(\text{Fe}_{0.97-x}\text{Co}_{0.03}\text{Cu}_x)\text{As}$ . The dashed lines represent the linear extrapolations of the normal state data to zero temperature. (b) DC magnetization of  $\text{Na}(\text{Fe}_{0.97-x}\text{Co}_{0.03}\text{Cu}_x)\text{As}$ .

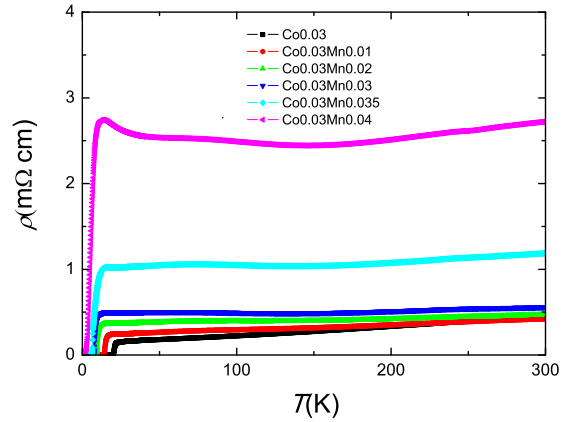


FIG. 5: (color online) Temperature dependence of the in-plane resistivity of  $\text{Na}(\text{Fe}_{0.97-x}\text{Co}_{0.03}\text{Mn}_x)\text{As}$ .

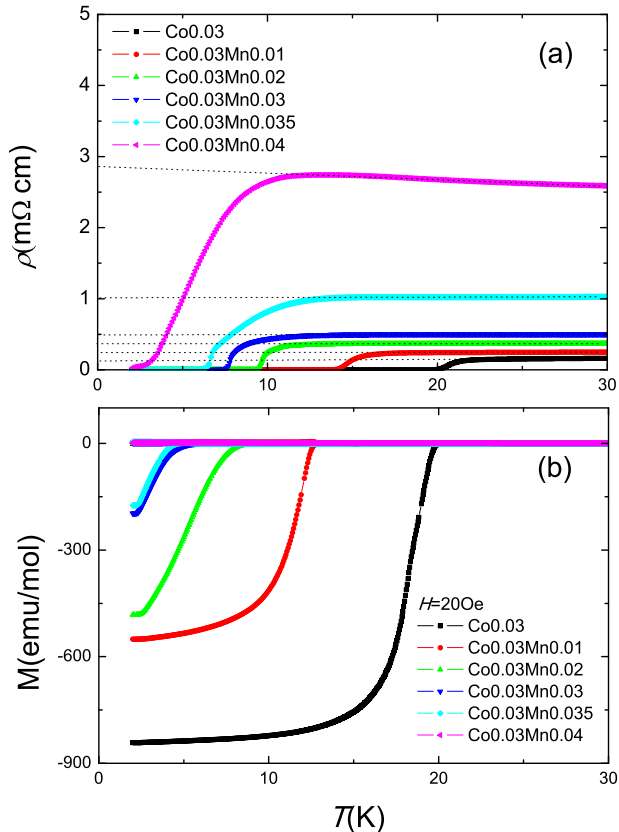


FIG. 6: (color online) (a) The resistivity curve in low temperature region for  $\text{Na}(\text{Fe}_{0.97-x}\text{Co}_{0.03}\text{Mn}_x)\text{As}$ . The dashed lines represent the linear extrapolation of the normal state data to zero temperature. (b) DC magnetization of a  $\text{Na}(\text{Fe}_{0.97-x}\text{Co}_{0.03}\text{Mn}_x)\text{As}$  single crystal.

increase of Cu concentration. In the low doping region, the resistivity decreases upon cooling, followed by a superconducting transition. For the highly doped sample, an upturn is observed at low temperatures. It is interesting to note that, for the sample  $x = 0.03$ , the transition seems to be broad, an initial drop of resistivity starts at about 16 K, which is followed by a sharper drop at about 8-9 K. This may be induced by a chemical segregation. But the strange point is that this broadened transition occurs in most of the measured curves of this doping level, even from the samples of different batches. We notice that, actually the normal state starts to show a low- $T$  upturn at this doping point. The low- $T$  upturn gets stronger with the increase of Cu content, which may be induced by a stronger localization effect. A strong semiconducting like temperature dependence of resistivity is observed on the sample with  $x=0.05-0.06$ . Interestingly, it is found that  $T_c$  is suppressed to zero at the threshold of strong semiconducting behavior. For the sample with

$x=0.05$ , a downward trend of resistivity is observed at about 2.5 K. So the doping level  $x=0.05$  is regarded as the critical doping concentration which suppresses  $T_c$  to zero. We define the residual resistivity  $\rho_0$  by extrapolating normal state data in a linear way in the low temperature region to zero temperature, as shown in Fig. 4(a). One can see,  $T_c$  decreases monotonously with the increase of  $\rho_0$ , and it is suppressed to zero at a residual resistivity of 0.87 m $\Omega$  cm. Fig. 4(b) shows the temperature dependence of DC magnetization taken at 20 Oe after the zero-field-cooling (ZFC) and field-cooling (FC) procedure for the superconducting  $\text{Na}(\text{Fe}_{0.97-x}\text{Co}_{0.03}\text{Cu}_x)\text{As}$  single crystals. In this study,  $T_c$  is defined on the magnetization curve using the crossing point of the normal state background line and the extrapolated linear line of the steep transition, which is nearly consistent with the point where resistivity reaches zero. For the pristine sample,  $T_c$  reaches about 20.5 K.

The temperature dependence of the in-plane resistivity and DC magnetization of  $\text{Na}(\text{Fe}_{0.97-x}\text{Co}_{0.03}\text{Mn}_x)\text{As}$  are shown in Fig. 5 and Fig. 6 (b), respectively. Same as the Cu-doped samples, the residual resistivity is determined by a linear extrapolation of normal state data to zero temperature, as shown in Fig. 6(a). It is clear that the residual resistivity increases with increasing the doping level, and consequently  $T_c$  is also suppressed monotonically. Interestingly, a similar broadening effect of resistivity as the case of doping Cu occurs at about  $x=0.035$ , which seems to be some kind of intrinsic feature. Compared with Cu doped samples, Mn doped ones show much weaker localization even to a very high doping, and the enhancement of residual resistivity changes from a slow speed to a fast one. Interestingly, superconductivity still exists in the sample with a residual resistivity even up to 2.86 m $\Omega$  cm. One may argue that the Mn dopants may not be successfully doped into the system when the concentration is higher than a certain value. However, this argument cannot be supported by the doping dependence of the  $c$ -axis lattice constant, as shown in Fig. 2(c). Moreover, the residual resistivity of the Mn doped samples increases also continuously, which again indicates a successful doping of Mn into the material. Clearly, the Mn impurity shows weaker  $T_c$  suppression effect than Cu in the high doping regime. This remains to be an interesting and unresolved observation.

### C. DC magnetization and analysis

In order to study the impurity scattering mechanism, it is crucial to determine whether the impurity is magnetic or nonmagnetic. To evaluate the magnetic moments induced by Cu and Mn dopants, we have done the magnetization measurements under high magnetic fields. The raw data of magnetization measurements at 1 T are shown in Fig. 7(a). The clear divergence of the magnetic susceptibility at low temperatures can be understood as the existence of some local magnetic moments.

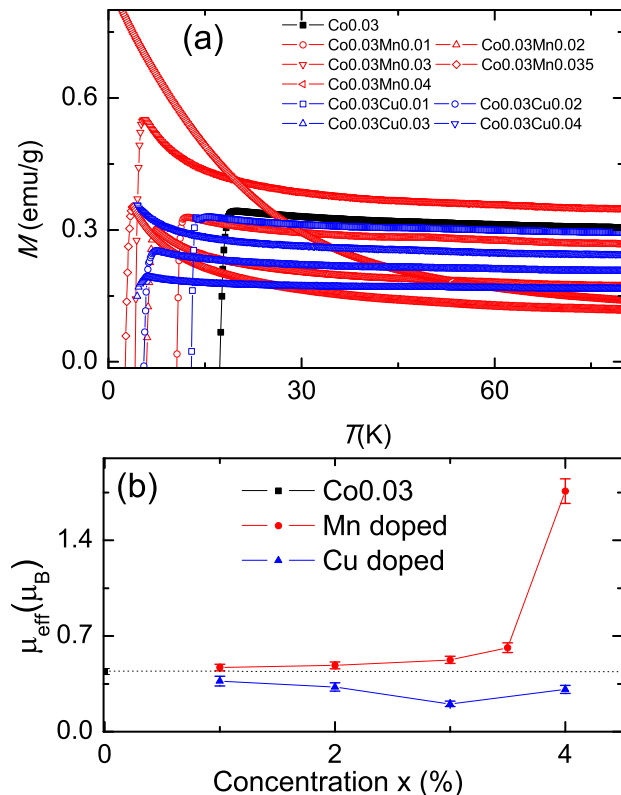


FIG. 7: (color online) (a) The magnetization measured at  $\mu_0 H = 1$  T on the pristine sample (black squares), the Cu doped samples (blue symbols) and the Mn doped samples (red symbols). One can see that the low temperature upturn gets enhanced clearly by the Mn doping, but not enhanced by the Cu doping. (b) The average magnetic moment per Fe site calculated by the Curie-Weiss law for the Cu and Mn doped samples. Clearly, doping Mn induces strong averaged magnetic moments, while doping Cu seems to weaken the averaged local magnetic moments.

One can see that the low temperature upturn gets enhanced clearly by the Mn doping, but not enhanced by the Cu doping, indicating that Mn is the magnetic impurity, while Cu behaves as non- or very weak magnetic impurity. To further investigate the magnetic moments induced by Cu and Mn dopants, we assume that the low temperature magnetization can be written in the Curie-Weiss law,

$$\chi = M/H = \chi_0 + C_0/(T + T_\theta), \quad (1)$$

where  $C_0 = \mu_0 \mu_{\text{eff}}^2 / 3k_B$ ,  $\chi_0$  and  $T_\theta$  are the fitting parameters,  $\mu_{\text{eff}}$  is the local magnetic moment per Fe site. The first term  $\chi_0$  comes from the Pauli paramagnetism of the conduction electrons, which is related to the density

of states (DOS) at the Fermi energy. The second term  $C_0/(T + T_\theta)$  is given by the local magnetic moments of the ions at the Fe sites (including dopants like Co, Cu, and Mn). The fitting process is not straightforward, for a precise evaluation on the local magnetic moments, we adjust the  $\chi_0$  value to get a linear function of  $1/(\chi - \chi_0)$  versus  $T$  in the low temperature limit. Then we fit the data with a linear function, as shown in Fig.8. The slope of the linear line gives  $1/C_0$ , and the intercept delivers the value of  $T_\theta/C_0$ . Once  $C_0$  is obtained, we can get the average magnetic moment of a single Fe site (including the contribution of Fe and the dopants). The results are shown in Fig. 7(b). Clearly, doping Mn induces strong local magnetic moments, while doping Cu seems to even weaken the average local moments. These facts suggest that Mn ions here play as a role of magnetic impurities, while Cu dopants act as the non- or weak magnetic impurities. One possible picture to interpret this is that the Cu dopant may have a full shell of  $d^{10}$  configuration with the ionic state of  $\text{Cu}^{1+}$  as predicted by the theoretical calculations.<sup>36,37</sup> Similar results are observed in Cu-doped  $\text{Fe}_{1+y}\text{Te}_{0.6}\text{Se}_{0.4}$ .<sup>32</sup>

#### D. Discussions

The residual resistivity of  $\text{Na}(\text{Fe}_{0.97-x}\text{Co}_{0.03}\text{T}_x)\text{As}$  ( $T=\text{Cu, Mn}$ ) plotted as a function of doping concentration  $x$  is shown in Fig. 9. One can see that both doping Cu and Mn can enhance the residual resistivity. In the low doping region ( $x=1\%, 2\%, 3\%$ ), the residual resistivity increases with the same ratio of  $0.18 \text{ m}\Omega \text{ cm}/\%$  for both Cu- and Mn-doped samples. However, the residual resistivity increases rapidly for highly Mn doped samples. Surprisingly, superconductivity still exists even up to a residual resistivity of  $2.86 \text{ m}\Omega \text{ cm}$  for the case of Mn doping. Similar phenomenon is observed in Co-doped  $\text{Fe}_{1+y}\text{Te}_{0.6}\text{Se}_{0.4}$  superconductor,<sup>32</sup> where superconductivity maintains even up to a residual resistivity of  $6 \text{ m}\Omega \text{ cm}$ . We must emphasize that the Mn elements have been doped into the Fe sites without doubt, because the lattice constant changes monotonously, and the high residual resistivity increases monotonously with the doping level of Mn up to 4%. For a simple  $S^\pm$  pairing model, this is very difficult to understand. A further in-depth understanding is highly desired.

In above we have discussed the influence of doping Cu and Mn on the lattice parameter, magnetization and resistivity. We have also discovered that Mn can enhance the local magnetic moments greatly, whereas Cu behaves as a nonmagnetic impurity. Based on these results, in the following, we focus on the discussion of pair-breaking mechanism for  $\text{Na}(\text{Fe}_{0.97-x}\text{Co}_{0.03}\text{T}_x)\text{As}$  ( $T=\text{Cu, Mn}$ ) superconductors. According to the  $S^\pm$  scenario with equal gaps of opposite signs on different Fermi surfaces,  $T_c$  is expected to be markedly suppressed due to potential scattering by substituted nonmagnetic impurities, and it obeys a universal Abrikosov-Gor'kov

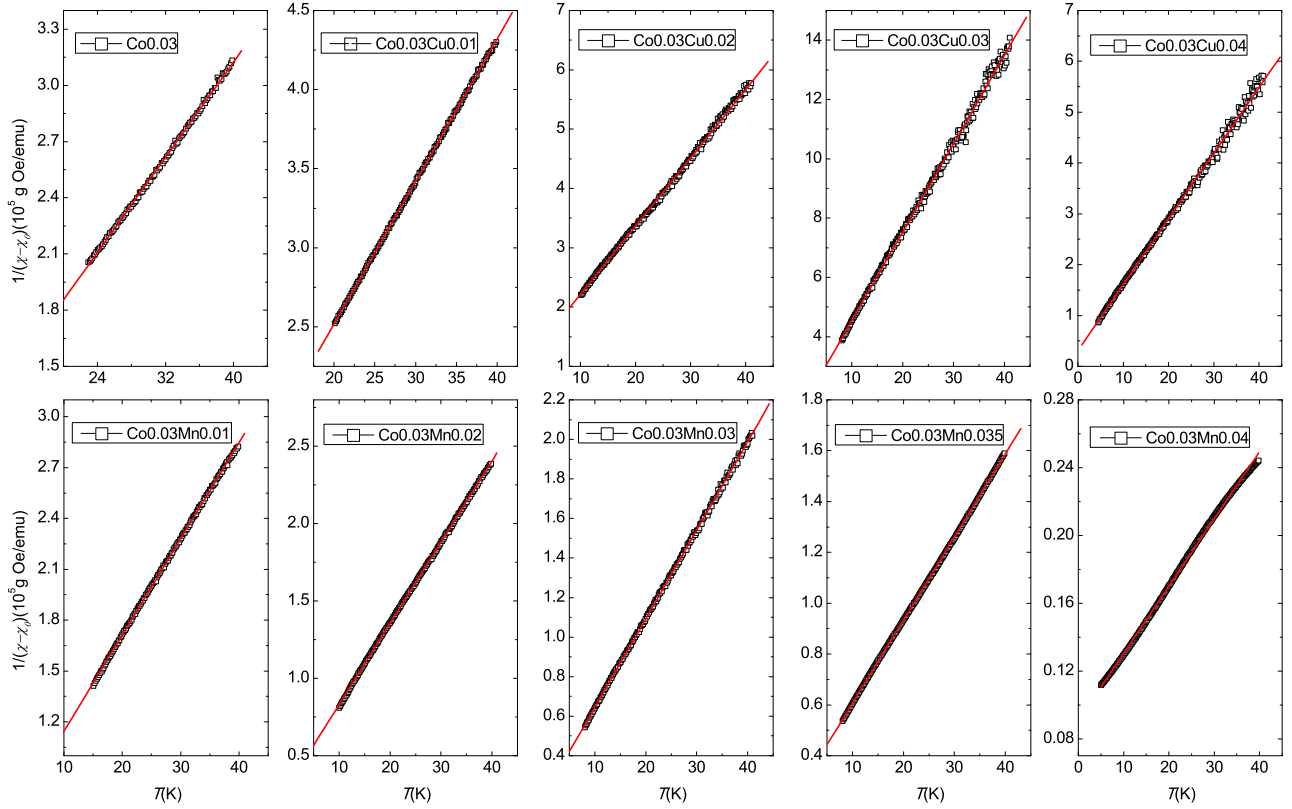


FIG. 8: (color online) Temperature dependence of  $1/(\chi-\chi_0)$  for  $\text{Na}(\text{Fe}_{0.97}\text{Co}_{0.03})\text{As}$  and  $\text{Na}(\text{Fe}_{0.97-x}\text{Co}_{0.03}\text{T}_x)\text{As}$  ( $\text{T} = \text{Cu}$  and  $\text{Mn}$ ) single crystals under 1 T with  $\chi$  the DC magnetic susceptibility. By adjusting  $\chi_0$  we obtain a linear relation of  $1/(\chi-\chi_0)$  with temperature in the low temperature limit. The red lines represent the linear fits of the data. The slope gives  $1/C_0$  and the intercept provides the value of  $T_\theta/C_0$ .

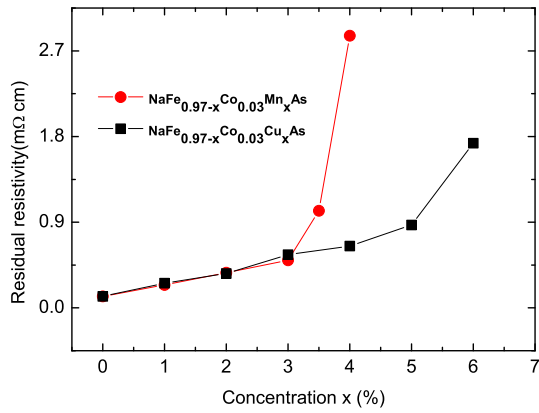


FIG. 9: (color online) Residual resistivity of  $\text{Na}(\text{Fe}_{0.97-x}\text{Co}_{0.03}\text{T}_x)\text{As}$  ( $\text{T} = \text{Cu}, \text{Mn}$ ) plotted as a function of doping concentration  $x$ .

formula,<sup>5</sup>  $-\ln t = \psi(1/2 + \alpha/2t) - \psi(1/2)$ , where  $t = T_c/T_{c0}$  with  $T_{c0}$  and  $T_c$  the transition temperatures of the pristine and the doped samples respectively,  $\psi(x)$  is the digamma function,  $\alpha$  is the pair breaking parameter.<sup>38</sup> The Abrikosov-Gor'kov formula would lead to that  $T_c$  vanishes at  $\alpha_c^{theory} = 0.28$ . However, plenty of previous studies of the impurity effect on the iron-based superconductor have revealed that the critical value of  $\alpha$  is much larger than 0.28, which means that the rate of  $T_c$  suppression found previously is too small to be explained by the  $S^\pm$  scenario.<sup>23-26,28,34</sup> According to the theoretical calculations based on the five-orbital model,<sup>11</sup>  $\alpha = z\hbar\Gamma/2\pi k_B T_{c0}$ , where  $z = m/m^*$  is the renormalization factor,  $\Gamma$  is the scattering rate. We use the relation  $\Gamma = ne^2\Delta\rho_0/m^* = e\Delta\rho_0/m^*R_H$ , where  $n$  is the carrier density,  $R_H$  is the Hall coefficient,  $m^*$  is the effective mass. In this study, we use  $z = 1/4.2$  obtained from optical spectroscopy experiment for Na-111 superconductor,<sup>39,40</sup>  $R_H = -7 \times 10^{-9} \text{ m}^3/\text{C}$  is obtained from the transport measurements by extrapolating  $R_H$  data to zero temperature,

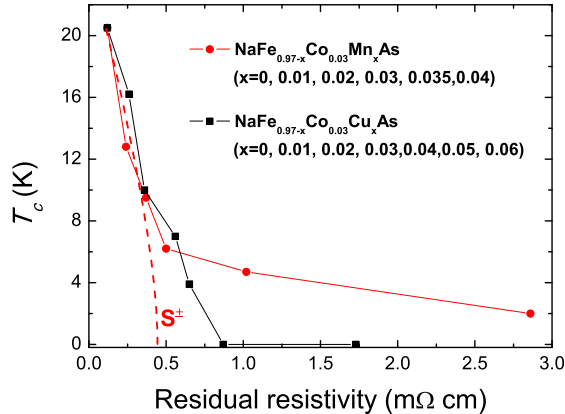


FIG. 10: (color online) Correlations between  $T_c$  and the residual resistivity for the investigated samples. The red dashed line represents the relationship between  $T_c$  and residual resistivity based on the  $S^\pm$  scenario, which is calculated using the relation  $\rho_0 = 2\pi\alpha k_B m^* R_H T_{c0} / z\hbar e + \rho_0^{pri}$  and follows a universal Abrikosov-Gor'kov formula. Here  $\rho_0^{pri}$  represents the residual resistivity of the pristine sample.

which is consistent with the result reported before.<sup>35</sup> The obtained critical value of  $\alpha$  for  $T_c$  to vanish based on our experimental data of Cu-doped sample is about 0.64, which is still much larger than the theoretically expected value  $\alpha_c = 0.28$ , but the gap between the experimental and the theoretical value becomes much smaller compared with the previous studies in the Ba122 system.<sup>24–26</sup>

To further study the pair-breaking mechanism in  $\text{Na}(\text{Fe}_{0.97-x}\text{Co}_{0.03}\text{T}_x)\text{As}$  ( $\text{T}=\text{Cu}, \text{Mn}$ ) system, we calculated the critical residual resistivity for  $T_c$  to vanish based on the  $S^\pm$  scenario, which is proportional to pair breaking parameter  $\alpha$ . The relationship between  $T_c$  and  $\alpha$  can be transformed into the relationship between  $T_c$  and residual resistivity by using the relation  $\rho_0 = 2\pi\alpha k_B m^* R_H T_{c0} / z\hbar e + \rho_0^{pri}$ , here  $\rho_0^{pri}$  represents the residual resistivity of the pristine sample. As shown in Fig. 10,  $T_c$  is plotted as a function of  $\rho_0$ . The dashed line represents the relationship between  $T_c$  and residual resistivity based on the  $S^\pm$  scenario, which follows a universal Abrikosov-Gor'kov formula. One can see that, the critical residual resistivity for  $T_c$  to vanish in the  $S^\pm$  model is 0.44 mΩ cm. As we can see, in the low doping region, our data can be roughly fitted to this model, which means

that the impurity effect in  $\text{Na}(\text{Fe}_{0.97}\text{Co}_{0.03})\text{As}$  induced either by Mn or Cu can be explained by the  $S^\pm$  scenario in the low doping regime. In the case of Mn doping, the behavior of suppression to  $T_c$  changes from a fast speed to a slow one and keeps the superconductivity even up to a residual resistivity of 2.86 mΩ cm, indicating that the magnetic Mn impurities are even not as detrimental as the non-magnetic Cu impurities to superconductivity in the high doping region. This is an interesting observation, further theoretical and experimental efforts are expected to carry out why the superconductivity can be so robust with the Mn doping.

#### IV. CONCLUSION

In summary, we studied the impurity effect in single crystals of  $\text{Na}(\text{Fe}_{0.97-x}\text{Co}_{0.03}\text{T}_x)\text{As}$  ( $\text{T}=\text{Cu}, \text{Mn}$ ). Analysis of DC magnetization based on the Curie-Weiss law indicates that, Mn doping gives magnetic impurity, whereas Cu dopants behave as non- or very weak magnetic impurities. However, it is found that both doping Cu and Mn can enhance the residual resistivity and suppress the superconductivity in the same rate in the low doping region, being consistent with the prediction of the  $S^\pm$  model. For the Cu-doped system, the superconductivity is suppressed completely at a residual resistivity of 0.87 mΩ cm, when a strong localization effect is observed. However, in the case of Mn doping, the behavior of suppression to  $T_c$  changes from a fast speed to a slow one and superconductivity survives even up to a residual resistivity of 2.86 mΩ cm. Clearly the magnetic Mn impurities are even not as detrimental as the non-magnetic Cu impurities to superconductivity in  $\text{Na}(\text{Fe}_{0.97}\text{Co}_{0.03})\text{As}$  system in the high doping regime.

#### Acknowledgments

We appreciate the useful discussions with Peter Hirschfeld, Igor Mazin. This work is supported by the Ministry of Science and Technology of China (973 Projects: No. 2011CBA001002, No. 2010CB923002, and No. 2012CB821403), the NSF of China, NCET project and PAPD.

\* hhwen@nju.edu.cn

<sup>1</sup> Y. Kamihara, T. Watanabe, M. Hirano, and H. Hosono, J. Am. Chem. Soc. **130**, 3296 (2008).

<sup>2</sup> C. C. Tsuei and J. R. Kirtley, Rev. Mod. Phys. **72**, 969 (2000).

<sup>3</sup> I. I. Mazin, D. J. Singh, M. D. Johannes, and M. H. Du, Phys. Rev. Lett. **101**, 057003 (2008).

<sup>4</sup> K. Kuroki, S. Onari, R. Arita, H. Usui, Y. Tanaka, H. Kon-

tani, and H. Aoki, Phys. Rev. Lett. **101**, 087004 (2008).

<sup>5</sup> A. V. Chubukov, D. V. Efremov, and I. Eremin, Phys. Rev. B **78**, 134512 (2008).

<sup>6</sup> F. Wang, H. Zhai, Y. Ran, A. Vishwanath, and D.-H. Lee, Phys. Rev. Lett. **102**, 047005 (2009).

<sup>7</sup> For a review, one can see P. J. Hirschfeld, M. M. Korshunov, and I. I. Mazin, Rep. Prog. Phys. **74**, 124508

- (2011).
- <sup>8</sup> T. Hanaguri, S. Niitaka, K. Kuroki, K. Takagi, *Science* **328**, 474 (2010).
  - <sup>9</sup> H. Yang, Z. Y. Wang, D. L. Fang, Q. Deng, Q. H. Wang, Y. Y. Xiang, Y. Yang, H. H. Wen, arXiv:1306.2001.
  - <sup>10</sup> A. D. Christianson, E. A. Goremychkin, R. Osborn, S. Rosenkranz, M. D. Lumsden, C. D. Malliakas, I. S. Todorov, H. Claus, D. Y. Chung, M. G. Kanatzidis, R. I. Bewley, and T. Guidi, *Nature* **456**, 930 (2008).
  - <sup>11</sup> S. Onari and H. Kontani, *Phys. Rev. Lett.* **103**, 177001 (2009).
  - <sup>12</sup> H. Kontani and S. Onari, *Phys. Rev. Lett.* **104**, 157001 (2010).
  - <sup>13</sup> T. Saito, S. Onari, and H. Kontani, *Phys. Rev. B* **82**, 144510 (2010).
  - <sup>14</sup> S. Maiti, M. M. Korshunov, T. A. Maier, P. J. Hirschfeld, and A. V. Chubukov, *Phys. Rev. Lett.* **107**, 147002 (2011).
  - <sup>15</sup> A. F. Wang, S. Y. Zhou, X. G. Luo, X. C. Hong, Y. J. Yan, J. J. Ying, P. Cheng, G. J. Ye, Z. J. Xiang, S. Y. Li, X. H. Chen, arXiv:1206.2030 (2012).
  - <sup>16</sup> P. W. Anderson, *J. Phys. Chem. Solids* **11**, 26 (1959).
  - <sup>17</sup> H. Alloul, J. Bobroff, M. Gabay, and P. J. Hirschfeld, *Rev. Mod. Phys.* **81**, 45 (2009).
  - <sup>18</sup> M.-H. Julien, T. Feher, M. Horvatic, C. Berthier, O. N. Bakharev, P. Sgransan, G. Collin, and J.-F. Marucco, *Phys. Rev. Lett.* **84**, 3422 (2000).
  - <sup>19</sup> G. Xiao, M. Z. Cieplak, A. Gavrin, F. H. Streitz, A. Bakhshai, and C. L. Chien, *Phys. Rev. Lett.* **60**, 1446 (1988).
  - <sup>20</sup> Y.-Y. Zhang, C. Fang, X. Zhou, K. Seo, W. F. Tsai, B. A. Bernevig, and J. Hu, *Phys. Rev. B* **80**, 094528 (2009).
  - <sup>21</sup> C. Tarantini, M. Putti, A. Gurevich, Y. Shen, R. K. Singh, J. M. Rowell, N. Newman, D. C. Larbalestier, P. Cheng, Y. Jia, and H. H. Wen, *Phys. Rev. Lett.* **104**, 087002 (2010).
  - <sup>22</sup> P. Cheng, B. Shen, J. P. Hu, and H. H. Wen, *Phys. Rev. B* **81**, 174529 (2010).
  - <sup>23</sup> P. Cheng, B. Shen, F. Han, and H. H. Wen, arXiv:1304.4568 (2013).
  - <sup>24</sup> J. Li, Y. F. Guo, S. B. Zhang, J. Yuan, Y. Tsujimoto, X. Wang, C. I. Sathish, Y. Sun, S. Yu, W. Yi, K. Yamaura, E. Takayama-Muromachi, Y. Shirako, M. Akaogi, and H. Kontani, *Phys. Rev. B* **85**, 214509 (2012).
  - <sup>25</sup> J. Li, Y. Guo, S. Zhang, Y. Tsujimoto, X. Wang, C. I. Sathish, S. Yu, K. Yamaura, and E. Takayama-Muromachi, *Solid State Commun.* **152**, 671 (2012).
  - <sup>26</sup> J. Li, Y. Guo, S. Zhang, S. Yu, Y. Tsujimoto, H. Kontani, K. Yamaura, and E. Takayama-Muromachi, *Phys. Rev. B* **84**, 020513 (2011).
  - <sup>27</sup> A. Günther, J. Deisenhofer, Ch Kant, H-A Krug von Nidda, V. Tsurkan, and A. Loidl, *Supercond. Sci. Technol.* **24**, 045009 (2011).
  - <sup>28</sup> T. Inabe, T. Kawamata, T. Noji, T. Adachi, and Y. Koike, *J. Phys. Soc. Jpn.* **82**, 044712 (2013).
  - <sup>29</sup> Y. Li, J. Tong, Q. Tao, C. Feng, G. Cao, W. Chen, and F. Zhang, *Z. Xu, New J. Phys.* **12**, 083008 (2010).
  - <sup>30</sup> D. Tan, C. Zhang, C. Xi, L. Ling, L. Zhang, W. Tong, Y. Yu, G. Feng, H. Yu, L. Pi, Z. Yang, S. Tan, and Y. Zhang, *Phys. Rev. B* **84**, 014502 (2011).
  - <sup>31</sup> Y. F. Guo, Y. G. Shi, S. Yu, A. A. Belik, Y. Matsushita, M. Tanaka, Y. Katsuya, K. Kobayashi, I. Nowik, I. Felner, V. P. S. Awana, K. Yamaura, and E. Takayama-Muromachi, *Phys. Rev. B* **82**, 054506 (2010).
  - <sup>32</sup> Z. T. Zhang, Z. R. Yang, L. Li, L. S. Ling, C. J. Zhang, L. Pi and Y. H. Zhang, *J. Phys.: Condens. Matter* **25**, 035702 (2013).
  - <sup>33</sup> R. Frankovsky, H. Luetkens, F. Tambornino, A. Marchuk, G. Pascua, A. Amato, H. Klauss, and D. Johrendt, *Phys. Rev. B* **87**, 174515 (2013).
  - <sup>34</sup> K. Kirshenbaum, S. R. Saha, S. Ziemak, T. Drye, and J. Paglione, *Phys. Rev. B* **86**, 140505 (2012).
  - <sup>35</sup> A. F. Wang, X. G. Luo, Y. J. Yan, J. J. Ying, Z. J. Xiang, G. J. Ye, P. Cheng, Z. Y. Li, W. J. Hu, and X. H. Chen, *Phys. Rev. B* **85**, 224521 (2012).
  - <sup>36</sup> S. Chadov, D. Schärff, G. H. Fecher, C. Felser, L. Zhang, and D. J. Singh, *Phys. Rev. B* **81**, 104523 (2010).
  - <sup>37</sup> H. Wadati, I. Elfimov, and G. A. Sawatzky, *Phys. Rev. Lett.* **105**, 157004 (2010).
  - <sup>38</sup> A. A. Abrikosov and L. P. Gor'kov: *Sov. Phys. JETP* **21**, 1243 (1961).
  - <sup>39</sup> Z. P. Yin, K. Haule and G. Kotliar, *Nature Mater.* **10**, 932 (2011).
  - <sup>40</sup> W. Z. Hu, G. Li, P. Zheng, G. F. Chen, J. L. Luo, and N. L. Wang, *Phys. Rev. B* **80**, 100507 (2009).
  - <sup>41</sup> Sangwon Oh, A. M. Mounce, Jeongseop A. Lee, W. P. Halperin, C. L. Zhang, S. Carr, and Pengcheng Dai, *Phys. Rev. B* **87**, 174517 (2013).